CrystEngComm

COMMUNICATION

Enhanced photoelectrochemical activity of nanostructured ZnFe$_2$O$_4$ thin films prepared by the electrospray technique†

Meng Wang, Yu Sun, Huanwen Chen, Yuan Zhang, Xiaofeng Wu, Keke Huang and Shouhua Feng*

Nanostructured spinel zinc ferrite (ZnFe$_2$O$_4$) thin films were prepared, using the electrospray technique, as photoabsorber material for photoelectrochemical water splitting. An enhanced photocurrent of 53 μA cm^{-2} at 1.23 V *versus* RHE was achieved, which is among the best results obtained for unmodified ZnFe$_2$O$_4$ photoanodes.

1. Introduction

In recent years, photoelectrochemical (PEC) water splitting has attracted great attention, due to its ability to convert solar energy into chemical energy in the form of storable hydrogen. Metal oxide semiconductors such as Fe$_2$O$_3$,[1–3] TiO$_2$[4,5] and BiVO$_3$[6,7] were used as photoelectrodes that oxidize water on the working electrode. However, these traditional photoelectrode materials have numerous limitations, such as inappropriate optical band gaps and poor electric properties, which have been considered as serious barriers to obtaining high solar-to-hydrogen conversion efficiency.[8,9] An ideal photo electrode should possess a narrow band gap, proper band potential, stable and economic chemical components and high energy conversion efficiency.[10] To fulfill these requirements, a lot of improvements have been achieved through modification of the structures and morphologies of these well-known semiconductors. However, we still need to search for a suitable photoelectrode material that is chemically stable and has a proper bandgap to absorb a larger fraction of the solar spectrum.

*State Key Laboratory of Inorganic Synthesis and Preparative Chemistry, College of Chemistry, Jilin University, Changchun 130012, P. R. China.
E-mail: shfeng@jlu.edu.cn*

Spinel ZnFe$_2$O$_4$ has been widely studied as a promising photoelectrode candidate, due to its narrow band gap of about 2.0 eV, low rate of surface recombination and low onset potential.[11] Usually, it is applied as a component of composites to efficiently improve the PEC performance of other well-known photoelectrode materials.[11–13] However, by itself, it has seldom been studied as a photoanode.[14–16] ZnFe$_2$O$_4$ is hardly used as a photoelectrode on a heat-sensitive transparent conductive oxide substrate, due to its high crystallization temperature.[17] In addition, the construction of nanostructures is a common and fruitful approach to improving the properties of photoelectrode materials, but for ZnFe$_2$O$_4$, this is still a challenge. Recently, Kim and co-workers reported the fabrication of ZnFe$_2$O$_4$ nanorod arrays by coating ZnO onto β-FeOOH nanorods. Although this kind of structure decreases the recombination of carriers to improve the photocurrent of the samples,[14,15] it is complex and difficult to operate. As a result, the preparation routes are of great importance in raising the PEC performance of ZnFe$_2$O$_4$ photoanodes.

Recently, the electrospray (ES) technique has been widely used in preparing nanostructured materials because the electrospray process produces highly discharged nano droplets, which have been used to provide a chemical reaction space to afford the nucleation and growth of the nanoparticles. Moreover, this method is simple, non-toxic, low cost, has high deposition efficiency and excellent control of morphology and stoichiometry.[18,19] In this paper, the ES technique is used to prepare the nanostructured semiconductor metal oxide ZnFe$_2$O$_4$ as a photoanode for PEC water splitting. The mixed solution is sprayed onto the FTO conducted substrate and then annealed in air at a relatively mild temperature. The effects of the synthesis parameters on the PEC performance of the ZnFe$_2$O$_4$ thin film are investigated through

the measurements of crystal structure, elemental components, and PEC characterizations. The optimized $ZnFe_2O_4$ film shows a water splitting photocurrent of ~53 μA cm^{-2} at 1.23 V *versus* RHE under standard illumination conditions (AM 1.5 G 100 mW cm^{-2}).

2. Experimental

2.1. Synthesis of ZnFe$_2$O$_4$ films

The spray solution was prepared by dissolving 0.3 M iron acetylacetonate and 0.15 M zinc nitrate in ethanol, which was sonicated to make it homogeneous. The $ZnFe_2O_4$ thin films were deposited using homemade equipment, including an injection pump (Kent Scientific Corporation, USA), a high voltage source (Boher High Voltage Power Supplies Co., Ltd, China), and a heater. The limit of the high voltage source was 15 kV because of its leakage at higher voltage. The precursor solution was pumped by a spray nozzle under high voltage to produce charged microdroplets. A pre-cleaned FTO substrate was placed against the nozzle to accept the charged microdroplets. The substrate was connected to a heater whose temperature was adjusted by a temperature controller. The distance between the tip of the needle and the substrate was fixed at 8.5 cm. The flow rate was maintained at 15 μL min^{-1}. After deposition, the films were annealed at 550 °C for 2 h to obtain crystalline $ZnFe_2O_4$.

2.2. Characterization

The morphological, structural and optical properties of the $ZnFe_2O_4$ thin films were characterized by using scanning electron microscopy (SEM, Helios Nanolab 600i from FEI Company), UV-vis spectroscopy (HITACHIU-4100), X-ray photoelectron spectroscopy (XPS), and X-ray diffraction (XRD, CuKα, 50 kV and 200 mA). Photoelectrochemical measurements were performed with a CHI802D electrochemical workstation (CH instruments Inc., Shanghai), using a three-electrode electrochemical cell. The $ZnFe_2O_4$ photoanodes were used as the working electrode, Ag/AgCl electrode as the reference electrode, and a platinum sheet as the counter electrode. The surface area exposed to the electrolyte was fixed at 0.502 cm^2, and 1 M aqueous solution of sodium hydroxide (pH = 13.6) was utilized as the electrolyte. The measured potentials *vs.* Ag/AgCl were converted to the reversible hydrogen electrode (RHE) scale, according to the relationship $E_{RHE} = E_{Ag/AgCl} + 0.059$ pH $+ E^0_{Ag/AgCl}$, where $E_{Ag/AgCl}$ is the measured potential against the reference electrode and $E^0_{Ag/AgCl} = 0.1976$ V at 25 °C. The scan rate was 10 mV s^{-1} for the current–potential (*J*–*E*) curves, and the scans were performed from negative to positive potentials. The light source was provided by a 500 W xenon lamp, and the light intensity was adjusted to 100 mW cm^{-2}.

3. Results and discussion

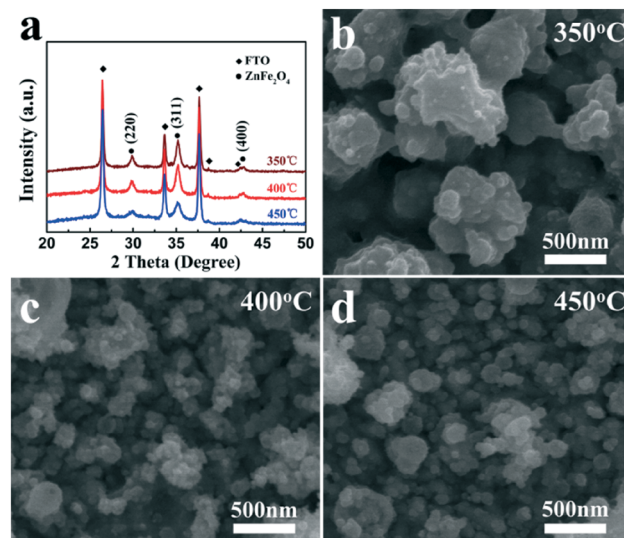The substrate temperature is commonly deemed as an important synthetic parameter for the growth of the oxide thin film

Fig. 1 (a) XRD patterns of $ZnFe_2O_4$ thin films prepared at different substrate temperatures. SEM images of films grown at different substrate temperatures: (b) 350 °C, (c) 400 °C and (d) 450 °C.

and its PEC performance. To investigate this effect, $ZnFe_2O_4$ thin films were deposited at 350 °C, 400 °C and 450 °C, and were labeled as ZFO1, ZFO2 and ZFO3, respectively. The XRD measurements were conducted to confirm the formation of $ZnFe_2O_4$ crystals, and the results are shown in Fig. 1(a). The peaks at 30°, 35.2° and 42.8° correspond to the (220), (311) and (400) crystal planes of $ZnFe_2O_4$, respectively. With an increase in substrate temperature, the (220) grain orientation diminished. This might be due to the different chemical reaction environments near the substrate. The discharged droplets were preheated and the oxidation reaction of the Fe precursor occurred at higher substrate temperature. A similar growth mechanism has been reported for a Fe_3O_4 thin film on the $SrTiO_3$ (001) substrate by Takahashi *et al.*,[20] and by
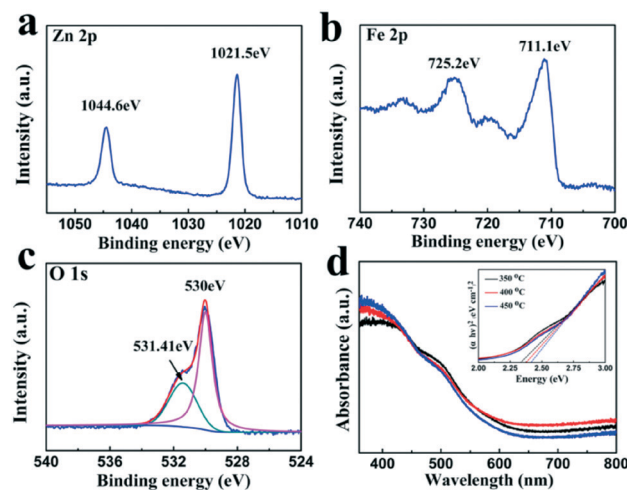

Fig. 2 (a) Zn 2p, (b) Fe 2p and (c) O 1s XPS spectra of $ZnFe_2O_4$ deposited at 350 °C; (d) UV-vis spectra of the $ZnFe_2O_4$ thin films, the inset shows the Tauc plots evaluating the optical band gaps.

Oh-Shim Joo *et al.* for α-Fe$_2$O$_3$ thin film on the FTO substrate.[21]

Fig. 2b–d show the SEM results of the films deposited at different substrate temperatures. An obvious variation in morphology can be observed. A lower temperature leads to a poorer nanostructure. However, with increasing the temperature, the film showed highly porous morphology. This is because the higher temperature of the plate heater results in higher temperature near the spray nozzle, which increases the evaporation rate of the solvent during the spraying process of droplets, resulting in smaller droplets, and consequently, smaller nanocrystals. The film consisted of small-sized nanoparticles and exposed more interfacial areas between ZnFe$_2$O$_4$ and the electrolyte, which increased its oxygen evolution activity. With a further increment in substrate temperature, the nanoparticles obviously aggregated and grew large. This may be caused by the Ostwald ripening mechanism. Based on these results, it is concluded that the substrate temperature has a great impact on the morphology of the films.

X-ray photoelectron spectroscopy was also performed to investigate the valence states and surface chemical compositions of the ZnFe$_2$O$_4$ samples and the results are summarized in Fig. 2a–c. In Fig. 2a, the two peaks with binding energies of around 1021.38 eV and 1044.54 eV are assigned to Zn 2p$_{3/2}$ and Zn 2p$_{1/2}$, respectively, indicating the Zn(II) oxidation state of ZnFe$_2$O$_4$. The two peaks centered at 725.2 eV and 711.1 eV are in good accordance with the Fe 2p$_{3/2}$ and Fe 2p$_{1/2}$, respectively. This result confirms that the Fe in ZnFe$_2$O$_4$ exists in the +3 oxidation state. In addition, the peaks at binding energies of ∼531.4 eV and ∼530.0 eV in Fig. 2c are ascribed to surface-absorbed oxygen species and typical surface lattice oxygen.

The optical properties of ZnFe$_2$O$_4$ thin film were investigated by UV-vis absorption spectroscopy, as shown in Fig. 2d. There is a rather broad absorption in a wide wavelength range from the UV to visible region, indicating that the ability of ZnFe$_2$O$_4$ for utilizing irradiated light is better than that of TiO$_2$. With the substrate temperature increasing, the band gap increases from 2.344 eV to 2.375 eV and 2.690 eV for ZFO1, ZFO2 and ZFO3, respectively (inset of Fig. 2d). The increase in the band gap may be due to the reduced oxygen vacancy concentrations resulting from the increased deposition temperature.[22]

The PEC performance of the films deposited at different temperatures was also investigated, as shown in Fig. 3. The photocurrent of the film prepared at 350 °C was only 6 μA cm^{-2} at 1.23 (V *vs.* RHE), and when deposited at 400 °C, it increased to 27 μA cm^{-2}, which was improved by about 4.5 times. The enhanced photocurrent can be attributed to the reduced grain size, which possessed a larger surface area and exposed more active sites. When the substrate temperature further increased, the photocurrent exhibited a small decrease. First, the poor crystallization, which was already indicated by the XRD patterns above, reduced the photocatalytic activity, due to the increased recombination probability.
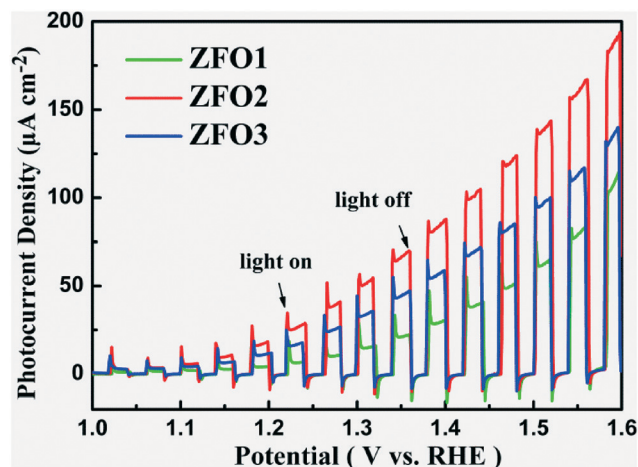

Fig. 3 Photocurrent-potential curves of ZnFe$_2$O$_4$ thin films prepared at different substrate temperatures.

Moreover, the larger nanoparticles also enlarged the diffusion distance of the carrier. As a result, the sample prepared at the substrate temperature of 400 °C showed the best oxygen oxidation activity. Therefore, we deposited films at 400 °C in the following experiments.

Additionally, the effects of film thickness and discharge potential on morphology and PEC performance of the films are also investigated. The results are shown in Fig. 4. The different thicknesses of ZnFe$_2$O$_4$ films were prepared by varying the amounts of the precursor solution. The cross-section SEM images are shown in Fig. S1.† The thicknesses of the films increased with the amount of precursor solution. As shown in Fig. 4(a), when the amount of precursor solution was 200 μL, the as-prepared film exhibited the highest photocurrent. With the amount further increasing, the photocurrent decreased. This was because the prepared film was too thin to produce enough carriers for the catalyst to carry on the reaction. Recombination of the photogenerated carriers took place first, resulting in the decrease in photocurrent.

The SEM images of the films deposited at different discharge potentials are shown in Fig. S2.† The nanoparticles became more dispersed and uniform with increased potential. A higher discharge potential made the discharged droplets break into much finer droplets, which led to a highly porous structure and enlarged the interfacial area between the ZnFe$_2$O$_4$ film and Pt electrolyte, producing more active sites.
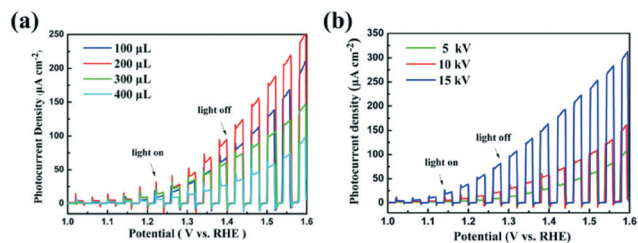

Fig. 4 Photocurrent-potential curves of ZnFe$_2$O$_4$ thin films prepared with different amounts of precursor solution (a) and discharge potential (b).

Fig. 4(b) depicts the photocurrent-potential curves of $ZnFe_2O_4$ thin films deposited at different potentials. The photocurrents increased with the discharge potentials. The film deposited at 15 kV showed the best oxygen evolution activity. According to the above results, higher potential produced highly porous thin films and exposed more active sites that could efficiently promote the oxygen evolution reaction. Meanwhile, the photogenerated holes were efficiently transformed on the surface of $ZnFe_2O_4$, which further oxidized OH^- to O_2 by reducing the electron–hole recombination. At 1.23 V (vs. RHE), the film showed a water splitting photocurrent density of ~53 $\mu A\ cm^{-2}$, which is among the best results obtained so far for unmodified $ZnFe_2O_4$ photoanodes.[14–16] At 1.6 V (vs. RHE), the photocurrent density was 331 $\mu A\ cm^{-2}$ before the flow of the dark current commenced.

4. Conclusions

In summary, zinc ferrite thin films were prepared on a transparent conductive substrate for water splitting, using the electrospray technique and post thermal treatment. Synthetic parameters, such as substrate temperature, film thickness and discharge potential, were optimized. The substrate temperature has a great influence on the PEC performance of $ZnFe_2O_4$ thin films. The film deposited at 400 °C showed the best water oxidation activity. The film thickness also played an important role in the PEC performance of $ZnFe_2O_4$ thin films. The thickness was optimized to obtain high water splitting activity. Highly porous thin films and an enlarged interfacial area between $ZnFe_2O_4$ and the electrolyte were obtained by increasing the discharge potential, producing more active sites and enhanced photocurrent. Therefore, we conclude that the electrospray technique is a facile route for preparing nanostructured photoanodes, and may be a promising route for preparing nanostructured materials for other applications such as gas sensing, Li-ion batteries, photochemical water purification and supercapacitors.

Acknowledgements

Notes and references

1   K. Kim, I. H. Kim, K. Y. Yoon, J. Lee and J. H. Jang, J. Mater. Chem. A, 2015, 3, 7706–7709.

2   J. Y. Kim, D. H. Youn, J. H. Kim, H. G. Kim and J. S. Lee, ACS Appl. Mater. Interfaces, 2015, 7, 14123–14129.

3   A. Kargar, S. J. Kim, P. Allameh, C. Choi, N. Park, H. Jeong, Y. Pak, G. Y. Jung, X. Pan, D. Wang and S. Jin, Adv. Funct. Mater., 2015, 25, 2609–2615.

4   X. Wei, X. F. Yang, A. Q. Wang, L. Li, X. Y. Liu, T. Zhang, C. Y. Mou and J. Li, J. Phys. Chem. C, 2012, 116, 6222–6232.

5   H. Cui, W. Zhao, C. Yang, H. Yin, T. Lin, Y. Shan, Y. Xie, H. Gu and F. Huang, J. Mater. Chem. A, 2014, 2, 8612–8616.

6   G. Li, D. Zhang and J. C. Yu, Chem. Mater., 2008, 20, 3983–3992.

7   J. Yu and A. Kudo, Adv. Funct. Mater., 2006, 16, 2163–2169.

8   H. J. Ahn, M. J. Kwak, J. S. Lee, K. Y. Yoon and J.-H. Jang, J. Mater. Chem. A, 2014, 2, 19999–20003.

9   Q. Peng, B. Kalanyan, P. G. Hoertz, A. Miller, D. H. Kim, K. Hanson, L. Alibabaei, J. Liu, T. J. Meyer, G. N. Parsons and J. T. Glass, Nano Lett., 2013, 13, 1481–1488.

10 P. Zhang, L. Gao, X. Song and J. Sun, Adv. Mater., 2015, 27, 562–568.

11 Y. F. Xu, H. S. Rao, X. D. Wang, H. Y. Chen, D. B. Kuang and C. Y. Su, J. Mater. Chem. A, 2016, 4, 5124–5129.

12 X. Li, C. Wang, H. Guo, P. Sun, F. Liu, X. Liang and G. Lu, ACS Appl. Mater. Interfaces, 2015, 7, 17811–17818.

13 X.-W. Hu, S. Liu, B. T. Qu and X. Z. You, ACS Appl. Mater. Interfaces, 2015, 7, 9972–9981.

14 J. H. Kim, J. H. Kim, J. W. Jang, J. Y. Kim, S. H. Choi, G. Magesh, J. Lee and J. S. Lee, Adv. Energy Mater., 2015, 5, 1401933.

15 J. H. Kim, Y. J. Jang, J. H. Kim, J. W. Jang, S. H. Choi and J. S. Lee, Nanoscale, 2015, 7, 19144–19151.

16 A. G. Hufnagel, K. Peters, A. Muller, C. Scheu, D. F. R. Ng and T. Bein, Adv. Funct. Mater., 2016, 26, 4435–4443.

17 K. Higashimine, K. Tajima and T. Mitani, Sci. Technol. Adv. Mater., 2007, 8, 282–285.

18 F. Zheng, D. Wang, H. Fang, H. Wang, M. Wang, K. Huang, H. Chen and S. Feng, Eur. J. Inorg. Chem., 2016, 2016, 1860–1865.

19 H. Fang, K. Huang, L. Yuan, X. Wu, D. Wang, H. Chen and S. Feng, New J. Chem., 2016, 40, 7294–7298.

20 R. Takahashi, H. Misumi and M. Lippmaa, Cryst. Growth Des., 2012, 12, 2679–2683.

21 G. Rahman and O. S. Joo, J. Mater. Chem. A, 2013, 1, 5554–5561.

22 M. Chakraborty, R. Thangavel, A. Biswas and G. Udayabhanu, CrystEngComm, 2016, 18, 3095–3103.